

Coupled BE-FE Scheme for Three-Dimensional Dynamic Interaction of a Transversely Isotropic Half-Space with a Flexible Structure

Morshedifard, A.¹ and Eskandari-Ghadi, M.^{2*}

¹ M.Sc., School of Civil Engineering, College of Engineering, University of Tehran, Tehran, Iran.

² Professor, School of Civil Engineering, College of Engineering, University of Tehran, Tehran, Iran.

Received: 02 Aug. 2016;

Revised: 05 Jan. 2017;

Accepted: 16 Jan. 2017

ABSTRACT: The response of structures bonded to the surface of a transversely isotropic half-space (TIHS) under the effect of time-harmonic forces is investigated using a coupled FE-BE scheme. To achieve this end, a Finite Element program has been developed for frequency domain analysis of 3D structures, as the first step. The half-space underlying the structure is taken into consideration using a Boundary Element technique that incorporates half-space surface load Green's functions for a transversely isotropic medium. Next, the two programs are combined using a direct coupling algorithm and the final program is obtained. To validate the results, some benchmark problems are solved with the FE and the BE programs, separately and then the coupled technique is checked with the results of some special cases for which the solutions are available in the literature. At the end, a parametric study is carried out on several common types of structures to study the effects of the degree of anisotropy of transversely isotropic soil medium on the dynamic behavior of the structure. Moreover, the effect of soil-structure interaction (SSI) on the natural vibration frequency of the structures is also studied.

Keywords: Boundary Element Method, Coupled BE-FE, Finite Element Method, Flexible Foundation, Soil-Structure-Interaction, Transversely Isotropic.

INTRODUCTION

Almost all structures are founded on deformable ground and it has been known for the past few decades that taking the dynamic response of the soil medium into account can have significant effects on the final design of the structure (Li et al., 2014). Over the years, this fact has encouraged researchers to take on the challenging task of exploring various analytical and numerical methods to address

the important problem of dynamic soil-structure interaction (SSI).

Most of the early research on SSI has been concerned with the problem of rigid foundations in contact with an isotropic half-space (see for example Luco and Westman, 1971; Awojobi and Grootenhuis, 1965). In these papers, the semi-analytical methods were utilized to obtain vertical, horizontal, torsional and rocking impedance and compliances of circular rigid foundations in contact with an isotropic half-space, as the

* Corresponding author E-mail: ghadi@ut.ac.ir

fundamental step in studying SSI. Since the natural soil deposits usually have a sedimentary character, their behavior can be best described by transversely isotropic constitutive laws. This fact has prompted researchers to extend the previously obtained analytical solutions for the isotropic half-space to a transversely isotropic half-space. For instance, Eskandari-Ghadi and Ardeshir-Behrestaghi (2010) solved the problem of a vibrating disc in an arbitrary depth of a TIHS and Eskandari-Ghadi et al. (2013) have, with the help of half-space Green's functions, investigated the vertical and horizontal harmonic vibrations of a rigid rectangular foundation attached on the top of a TIHS. Ardeshir-Behrestaghi et al. (2013), with the use of potential functions, obtained the dynamic response of a transversely isotropic, linearly elastic layer bonded to the surface of a TIHS under arbitrary shape surface load. Also, Eskandari-Ghadi et al. (2014), with introducing a function space, have numerically determined the vertical impedance function of a rigid circular plate rested on the top of a TIHS.

Since analytical solutions are only available for foundations with a simple geometry, we need to consider numerical methods for tackling more complicated engineering boundary value problems in SSI. The Finite Element and Boundary Element methods are two of such techniques. The Finite Element method, however, has an inherent deficiency in handling boundary value problems where a semi-infinite soil medium needs to be modeled since a truncation of the infinite domain at a finite distance from the disturbance is unavoidable. Various techniques such as energy absorbing boundaries (Nielsen, 2014) and non-reflecting boundary conditions (Givoli, 2004) have been utilized to indirectly incorporate the deleted portion of the semi-infinite medium. In all these methods, a portion of the soil medium should eventually be modeled

and it should be noted that it is rather complicated to come up with these techniques to handle the problem of wave propagation in a general anisotropic medium (Savadatti and Guddati, 2012a,b).

The Boundary Element method, on the other hand, is an excellent alternative to the Finite Element method for modeling the semi-infinite half-space. The Green's functions utilized in this method automatically satisfy the radiation condition at infinity and consequently there are no pollution of the results from reflected waves at the far boundaries (Aleynikov, 2010). However, the same Green's functions can also be viewed as the method's Achilles' heel since they can be very difficult to obtain in closed form for complex boundary value problems such as for anisotropic and non-homogeneous mediums. The Green's functions for a TIHS, can be found for example in the work of Eskandari-Ghadi and Amiri-Hezaveh (2014) and Akbari et al. (2016). In their solution, the governing equations for an exponentially graded medium have been uncoupled using a set of potential functions. Next, Fourier series and Hankel integral transforms have been used to arrive at the final expressions for displacement and stress fields in the semi-infinite exponentially graded medium.

Wong and Luco (1976) were among the first researchers to use constant Boundary Elements to evaluate the vertical, rocking and horizontal compliance functions for an arbitrary-shaped rigid structure resting on an isotropic half-space. More detailed expositions with attention to multilayered isotropic half-spaces can be found in Guzina (2000). In a similar research, Amiri-Hezaveh et al. (2013) have presented the horizontal and vertical impedance functions for a rigid rectangular foundation in contact with a transversely isotropic multilayered half-space using the same constant Boundary Elements. The scaled boundary Finite Element is also

another numerical method that can be applied for the solution of problems in dynamic SSI. Bazyar and Song (2006) applied the method for solution of the problem of either a rigid strip or square foundation embedded in a transversely isotropic non-homogeneous half-space.

All the above mentioned researches have focused on structures with infinite rigidity. If the flexibility of the foundation is taken into consideration, an analytical solution for the dynamic case becomes extremely formidable. Eskandari-Ghadi et al. (2015) have tried to investigate static interaction of flexible circular and annular plates with layered transversely isotropic half-space in detail, where they considered the possibility of separation of the flexible foundation from the half-space into account. Moreover, Gucunski and Peek (1993) solved the problem of vibration of an elastic circular plate attached on a multilayered medium. The plate discretization has been achieved by the Finite Difference energy method (Lima et al., 2014) and a ring element method has been used for the surface of the half-space. The dynamic interaction of a flexible rectangular plate with an isotropic medium was also investigated by Whittaker and Christiano (1982).

As mentioned previously, the BEM has a unique capability in modeling the domain of the semi-infinite media analytically; however the surface of the domain has to be considered numerically. On the other hand, the superstructure can be effectively modeled using the FEM. This complementarity nature of these two methods has been the drive behind the pioneering work of Zienkiewicz et al. (1977), where a combined FE-BE method was proposed for the first time. Since then, various coupling techniques such as iterative (Soares and Godinho, 2014) and direct (Coulier et al., 2014) methods have been proposed to achieve the desired coupling of the two numerical schemes. Moreover, Hematiyan et al. (2012) proposed a general

technique that can also be used for the BEM-FEM coupling. The main issue with regard to iterative methods, however, is their convergence. A discussion of the method and its convergence can be found in the work of Elleithy et al. (2001). Other methods such as overlapping domain decomposition method (see Elleithy and Al-Gahtani, 2000) and variational techniques (see Lu et al., 1991) can also be applied to achieve the coupling.

In the dynamic SSI, the application of some coupling techniques can be observed in the paper by Coulier et al. (2014) among others. An excellent comparison of the performance of several iterative methods and the direct coupling method in dynamic SSI is presented in their work and the accuracy of the direct coupling scheme is demonstrated. Moreover, Kokkinos and Spyarakos (1991) used the direct coupling method to investigate the problem of a flexible plate on the surface of an isotropic half-space. In their solution, both applied loads and seismic disturbances were considered in the frequency domain. We should also mention that coupling methods are not limited to the problems in SSI and applications in fracture mechanics can be found in the work of Frangi and Novati (2003).

To the best of the authors' knowledge, an accurate investigation of interaction of general three-dimensional flexible structures with a transversely isotropic half-space has not been carried out yet. In this paper, the direct coupling technique is used to investigate the frequency domain dynamic behavior of several types of structures that are bonded to the surface of a TIHS. In this way, we study the challenges due to interaction of structures of any stiffness with the soil described by transversely isotropic behavior, which is categorized in the soil-structure-interaction. The frequency domain Finite Element program that has been developed in this work for modeling the structure uses 20-node isoparametric brick elements and the

Boundary Element program prepared for this research uses 8-node quadratic elements that are compatible with the 20-node brick elements in the FE mesh of the structure. Regarding accuracy, using these elements makes the present work more accurate than many of the previous research done for rigid structures that have mainly used constant or linear elements for the mesh on the surface patch of the half-space in contact with rigid structures. Moreover, the half-space Green's functions derived in Eskandari-Ghadi and Amiri-Hezaveh (2014) have been presented in a concise manner and are used in the BE formulation of this work. The use of half-space Green's functions makes it possible to restrict the meshed area to the interface of the structure and the half-space in the BE program. Several cases have been chosen from the literature to demonstrate the validity and accuracy of the adopted method. The effects of variations of three different elastic parameters of the TIHS have also been studied for circular, rectangular and general structures to have a parametric study for the effect of degree of anisotropy of the half-space on the results of the SSI analysis for the first time. The results of this paper show that the anisotropy of the soil medium can have a significant effect on the natural vibration frequency of the structure and also the displacement magnitudes are noticeably affected.

It is also important to note that since we are considering the problem in Fourier space of frequency domain, the solution in the time domain can be obtained by applying the inverse Fourier transform to the results obtained herein, and thus the procedure used in this paper is restricted to the linear SSI

problems. This seems to be a prohibitive issue since soil deposits can show nonlinearity in the near field. The remedy is to model a portion of the near field along with the structure using the Finite Element method which is capable of capturing the nonlinear behavior. This method can be found in the work of Yazdchi et al. (1999).

NUMERICAL FORMULATION

A summary of the formulations for Finite Element and Boundary Element techniques, and the formulations for their combination is presented in this section. The Boundary Element method is described for the TIHS and a schematic of a typical problem is displayed in Figure 1. In this figure, Ω_f is the structure's domain modeled using Finite Elements, Ω_b represents the domain of the TIHS and Γ_I is the interface between the two domains.

Finite Element Formulation

Discretization of the structural domain (Ω_f) and applying the standard Finite Element technique leads to the following set of equations for a problem in linear elastodynamics (see Zienkiewicz et al. (2013) for more details):

$$\mathbf{M}\ddot{\mathbf{u}} + \mathbf{C}\dot{\mathbf{u}} + \mathbf{K}\mathbf{u} = \mathbf{f} \quad (1)$$

where \mathbf{M} is the mass matrix, \mathbf{C} is the matrix of material damping, \mathbf{K} is the stiffness matrix and the vectors $\ddot{\mathbf{u}}, \dot{\mathbf{u}}, \mathbf{u}$ and \mathbf{f} are the nodal accelerations, velocities, displacements and equivalent forces.

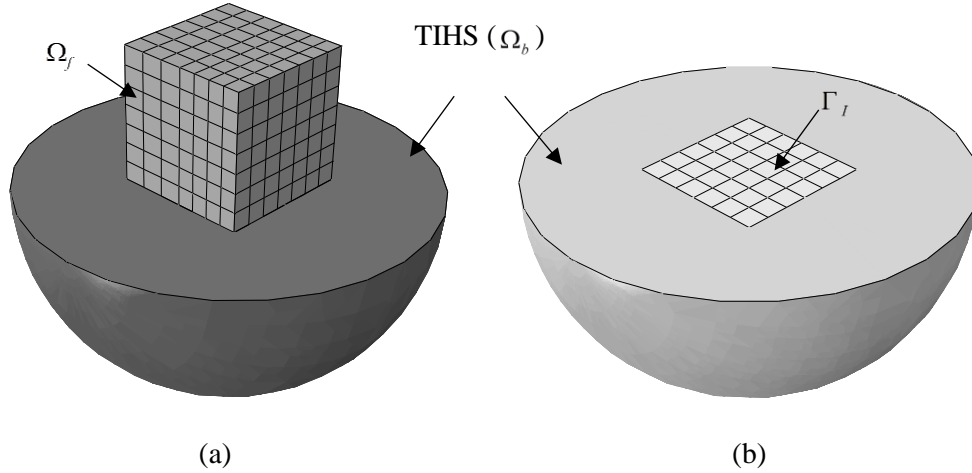


Fig. 1. a) A typical structure modeled by 3D Finite Elements attached to the TIHS, b) the structure's interface with the TIHS modeled with 8-node boundary elements

In the special case where the material damping is neglected and the applied force varies harmonically with time, Eq. (2) can be written as:

$$\mathbf{K}_f(\omega)\mathbf{u} = \mathbf{f}(\omega); \quad \mathbf{K}_f(\omega) = \mathbf{K} - \omega^2\mathbf{M} \quad (2)$$

where ω is the frequency of the external excitation and \mathbf{K}_f is the dynamic stiffness matrix for the structure.

Boundary Element Formulation for the Transversely Isotropic Half-Space

A good starting point for description of the direct Boundary Element method is the Boundary Integral Equation (BIE), which is used in the present work for the time-harmonic elastodynamic boundary value problem. The forces applied on the half-space are due to interaction of the super-structure that rests on the TIHS. Thus, assuming body forces to be negligible and also taking Γ_b to represent the boundary of the domain, we arrive at:

$$\mathbf{c}^i \mathbf{u}^i + \int_{\Gamma_b} \mathbf{p}^{*i}(\mathbf{x}, \omega) \mathbf{u}(\mathbf{x}, \omega) d\mathbf{x} = \int_{\Gamma_b} \mathbf{u}^{*i}(\mathbf{x}, \omega) \mathbf{p}(\mathbf{x}, \omega) d\mathbf{x} \quad (3)$$

where the superscript i represents an arbitrary point on the boundary of the domain and represents the source point. In this formulation, $\mathbf{p}(\mathbf{x}, \omega)$ and $\mathbf{u}(\mathbf{x}, \omega)$ are the traction and displacement vectors at $\mathbf{x} \in \Gamma_b$,

which is the field point and $\mathbf{c}^i = \mathbf{c}(\mathbf{x}_i)$ in the case of 3D elasticity is a 3×3 matrix representing the smoothness at point \mathbf{x}_i . $\mathbf{p}^{*i}(\mathbf{x}, \omega)$ and $\mathbf{u}^{*i}(\mathbf{x}, \omega)$ are the traction and displacement tensors when \mathbf{x}_i is taken as the source point and \mathbf{x} is the field point.

In the Boundary Element method, the boundary Γ_b is discretized into a number of 2D elements with some appropriate interpolation functions to be used to evaluate the integrals over each element, numerically. The components of the matrix \mathbf{c}^i are computed using a rigid body displacement for the domain under consideration. In this paper, since the fundamental solutions for the half-space are used, we arrive at:

$$\mathbf{c}^i = \mathbf{I} \quad (4)$$

where \mathbf{I} is the identity matrix (3×3 for 3D problems). Eq. (4) is compatible with the smoothness of the boundary of the half-space.

Moreover, use of half-space Green's functions makes the integral on the left hand side of Eq. (3) to be identically equal to zero. Considering the simplifications resulting from utilizing half-space Green's functions and assembly of the element matrices, we arrive at the following equation:

$$\hat{\mathbf{u}} = \mathbf{G}\hat{\mathbf{p}} \quad (5)$$

where $\hat{\mathbf{u}}$ and $\hat{\mathbf{p}}$ are the global boundary nodal displacements and tractions, respectively. The details of the Boundary Element solution are overlooked here for the sake of brevity.

Green's Tensor for a TIHS

The success of a Boundary Element solution for an engineering boundary value problem is highly dependent on the availability of Green's functions for the problem. The Green's functions, for a TIHS loaded by a time-harmonic point-load on its surface, can be derived with the use of a couple of complete scalar potential functions presented in Eskandari-Ghadi (2005). The solution is obtained in cylindrical coordinates and also involves a Fourier expansion in the angular direction and Hankel integral transforms in the radial direction. Consequently, we need to compute the inverse Hankel integral transforms to get the Green's functions for the half-space (see Eskandari-Ghadi and Amiri-Hezaveh (2014) for more details). We can express the displacement Green's functions at a point on the surface of the TIHS in the cylindrical coordinates resulting from application of a point load in each of the Cartesian directions on the surface of the half-space:

$$\begin{aligned} u_{xr} &= \cos(\theta) / (4\pi c_{44}) \\ &\quad (I_1 - I_2 + I_3 + I_4) \\ u_{xt} &= -\sin(\theta) / (4\pi c_{44}) \\ &\quad (I_1 + I_2 + I_3 - I_4) \\ u_{xz} &= -\cos(\theta) / (2\pi c_{44}) I_5; \\ u_{yr} &= \cos(\theta - \pi / 2) / (4\pi c_{44}) \\ &\quad (I_1 - I_2 + I_3 + I_4) \\ u_{yt} &= -\sin(\theta - \pi / 2) / (4\pi c_{44}) \\ &\quad (I_1 + I_2 + I_3 - I_4) \\ u_{yz} &= -\cos(\theta - \pi / 2) / (2\pi c_{44}) I_5; \\ u_{zr} &= 1 / (2\pi c_{44}) I_7; u_{zt} = 0; \\ u_{zz} &= 1 / (2\pi c_{44}) I_6; \end{aligned} \quad (6)$$

where u_{xr}, u_{xt} and u_{xz} are the displacement components in the r, θ and z directions at the field point on the surface of the half-space when a unit point-load is applied in the x direction at the source point on the surface of the TIHS. Similarly, u_{yr}, u_{yt} and u_{yz} are the displacement components when the point force is applied in the y direction and u_{zr}, u_{zt} and u_{zz} are the displacement components when the point load is applied in the z direction. All the integrals involved in these formulations may be written in the following compact form:

$$\begin{aligned} [I_1, I_2, I_3] &= \int_0^\infty [\xi\gamma_1(\xi)J_0(r\xi), \xi\gamma_1(\xi)J_2(r\xi), \xi\gamma_2(\xi)J_0(r\xi)] d\xi \\ [I_4, I_5, I_6] &= \int_0^\infty [\xi\gamma_2(\xi)J_2(r\xi), \xi\Omega_1(\xi)J_1(r\xi), \xi\Omega_2(\xi)J_0(r\xi)] d\xi \\ I_7 &= \int_0^\infty \xi\gamma_3(\xi)J_1(r\xi) d\xi \end{aligned} \quad (7)$$

where r is the norm of the position vector from point i (the source point) to \mathbf{x} (the field point) and the functions in the integrands are defined as:

$$\begin{aligned}
 \gamma_1(\xi) &= \frac{\alpha_3}{I(\xi)}(\nu_1\lambda_2 - \nu_2\lambda_1); \quad \gamma_2(\xi) = \frac{1}{\lambda_3} \\
 \gamma_3(\xi) &= \frac{\xi c_{44}\alpha_3}{c_{33}I(\xi)}(\eta_1\lambda_2 - \eta_2\lambda_1); \\
 \Omega_1(\xi) &= \frac{1+\alpha_1}{\xi I(\xi)} \left\{ \left[\frac{\rho_0\omega^2}{1+\alpha_1} - \xi^2 \right]^* \right. \\
 & \left. [v_1 - v_2] + \frac{\alpha_2}{1+\alpha_1} [v_1\lambda_2^2 - v_2\lambda_1^2] \right\} \\
 \Omega_2(\xi) &= \frac{-c_{44}(1+\alpha_1)}{c_{33}I(\xi)} \left\{ \left[\frac{\rho_0\omega^2}{1+\alpha_1} - \xi^2 \right]^* \right. \\
 & \left. [\eta_2 - \eta_1] + \frac{\alpha_2}{1+\alpha_1} [\eta_2\lambda_1^2 - \eta_1\lambda_2^2] \right\}
 \end{aligned} \tag{8}$$

The remaining parameters are:

$$\begin{aligned}
 \nu_i &= (\eta_i - \alpha_3 \frac{c_{13}}{c_{33}} \xi^2 - \alpha_3 \lambda_i^2) \lambda_i, \quad i = 1, 2 \\
 \eta_i &= (\alpha_3 - \alpha_2) \lambda_i^2 + \xi^2 (1 + \alpha_1) - \rho_0 \omega^2, \quad i = 1, 2 \\
 \lambda_{1,2} &= \sqrt{a\xi^2 + b \pm \frac{1}{2} \sqrt{c\xi^4 + d\xi^2 + e}}; \\
 I(\xi) &= \eta_2\nu_1 - \eta_1\nu_2 \\
 \lambda_3 &= \sqrt{s_0^2(\xi^2 - \rho_0\omega^2)}
 \end{aligned} \tag{9}$$

where we have:

$$\begin{aligned}
 a &= \frac{1}{2}(s_1^2 + s_2^2); \quad b = -\frac{1}{2}\rho\omega^2 \left(\frac{1}{c_{44}} + \frac{1}{c_{33}} \right); \\
 c &= (s_2^2 + s_1^2)^2 \\
 d &= -2\rho\omega^2 \left[\left(\frac{1}{c_{44}} + \frac{1}{c_{33}} \right) (s_1^2 + s_2^2) - 2 \frac{c_{11}}{c_{33}c_{44}c_{11}} \left(\frac{1}{c_{33}} + \frac{1}{c_{11}} \right) \right] \\
 e &= \rho^2\omega^4 \left(\frac{1}{c_{33}} - \frac{1}{c_{44}} \right)^2; \quad \alpha_1 = \frac{(c_{66} + c_{12})}{c_{66}}; \\
 \alpha_2 &= \frac{c_{44}}{c_{66}} \\
 \alpha_3 &= \frac{(c_{13} + c_{44})}{c_{66}}; \quad \rho_0 = \frac{\rho}{c_{66}}; \quad s_0 = \sqrt{\frac{1}{\alpha_2}}
 \end{aligned} \tag{10}$$

In these relations, c_{ij} and ρ are the elasticity constants for a transversely isotropic material and mass density, respectively. s_1 and s_2 are also the non-pure imaginary roots of the characteristic equation $c_{33}c_{44}s^4 + (c_{13}^2 + 2c_{13}c_{44} - c_{11}c_{33})s^2 + c_{11}c_{44} = 0$. The following relationships hold among the elasticity constants and the engineering parameters (Eskandari-Ghadi et al., 2012) :

$$\begin{aligned}
 c_{11} &= \frac{E(1 - \frac{E}{E'}\nu'^2)}{\frac{E'}{E'}}, c_{13} \\
 &= \frac{E\nu'}{1 - \nu - 2\frac{E}{E'}\nu'^2}, c_{44} = G', \\
 c_{33} &= \frac{E'(1 - \nu)}{1 - \nu - 2\frac{E}{E'}\nu'^2}, c_{66} \\
 &= \frac{E}{2(1 + \nu)} = G, c_{12} = c_{11} - 2c_{66}.
 \end{aligned} \tag{11}$$

where E and E' are Young's moduli in the plane of isotropy and in a direction normal to it, respectively. Poisson's ratios ν and ν' characterize the lateral strain response in the plane of transverse isotropy to a stress acting parallel and normal to it, respectively. G' and G are the shear moduli in the planes normal to the plane of transverse isotropy and in the plane of isotropy, respectively (Eskandari-Ghadi et al., 2012).

The components of the displacement Green's functions are needed in the Cartesian coordinates. Thus, we apply the transformation:

$$\mathbf{T} = \begin{pmatrix} \cos(\theta) & -\sin(\theta) & 0 \\ \sin(\theta) & \cos(\theta) & 0 \\ 0 & 0 & 1 \end{pmatrix} \tag{12}$$

on each of the three vector $\mathbf{v}_1 = [u_{xr}, u_{xt}, u_{xz}]^T$, $\mathbf{v}_2 = [u_{yr}, u_{yt}, u_{yz}]^T$ and $\mathbf{v}_3 = [u_{zr}, u_{zt}, u_{zz}]^T$. Finally, the Green's displacement tensor is obtained as

$$\mathbf{u}^* = \begin{pmatrix} (\mathbf{T}\mathbf{v}_1)^T \\ (\mathbf{T}\mathbf{v}_2)^T \\ (\mathbf{T}\mathbf{v}_3)^T \end{pmatrix} = \begin{pmatrix} u_{xr} \cos(\theta) - u_{xt} \sin(\theta) & u_{xr} \sin(\theta) + u_{xt} \cos(\theta) & u_{xz} \\ u_{xy} & u_{yr} \sin(\theta) + u_{yt} \cos(\theta) & u_{yz} \\ -u_{xz} & -u_{yz} & u_{zz} \end{pmatrix} \quad (13)$$

where we have taken advantage of the relations $u_{yx} = u_{xy}$, $u_{zx} = -u_{xz}$ and $u_{zy} = -u_{yz}$ which hold when half-space fundamental solutions are used. A closer look at the integrals in Eq. (7) reveals three major issues regarding their evaluation, which are (a) the upper limit is infinite, (b) there exist singularities on the path of integration, and (c) the existence of Bessel functions makes an oscillatory nature for the integrands. The methods presented by Longman are capable of handling these issues in a simple and elegant manner and we have taken advantage of them in the present work (Chen and An, 2014; Hamidzadeh et al., 2014).

Coupling Procedure

As explained in the previous sections, the dynamic stiffness matrix \mathbf{K}_f is determined using the Finite Element procedure, and the Boundary Element solution results in the matrix of influence coefficients, \mathbf{G} (Eqs. (2) and (5)). These matrices are of different natures and cannot be directly combined. Our objective is to convert the \mathbf{G} matrix from the BE solution to an FE-like matrix so that we can assemble the resulting matrix with the structure's stiffness matrix as if the half-space were a super element (Coulier et al., 2014). Consequently, we need to obtain a matrix \mathbf{Q}

that relates nodal tractions to nodal equivalent forces on the BE-FE interface:

$$\hat{\mathbf{f}} = \mathbf{Q}\hat{\mathbf{p}} \quad (14)$$

The global matrix \mathbf{Q} is obtained by assembly of local matrices for each element on the interface. Using isoparametric elements, we have:

$$\mathbf{Q}^e = \int_{-1}^1 \int_{-1}^1 \mathbf{\Phi}(s,t)^T \mathbf{\Phi}(s,t) J(s,t) ds dt \quad (15)$$

where $\mathbf{\Phi}(s,t)$ is the matrix of shape functions and $J(s,t)$ is the Jacobean of the transformation. Using Eqs. (14) and (5), we get the following stiffness matrix for the half-space:

$$\mathbf{K}_b = \mathbf{Q}\mathbf{G}^{-1} \quad (16)$$

NUMERICAL RESULTS

To carry out a numerical investigation, a combined BE-FE program has been developed in the MATLAB programming language according to the formulations presented in the previous sections. In the solutions procedure, 3D 20-node isoparametric brick elements are used for the FE mesh and a conforming mesh of 8-node 2D isoparametric elements are utilized for the TIHS. Moreover, 27 and 4 Gauss points are used for the integration of elements in the FE and BE programs, respectively. The mesh needed for modeling the structures are first created in the ABAQUS commercial software and then imported into the program as input. Needless to say, one may make the mesh for Finite Element part by himself. In what follows, we first demonstrate the accuracy and validity of the program prepared here by verifying the FE, BE and the combined parts, separately. It should be noted that only some special applications of the

general combined program can be compared with the available reported documents in the literature. At the end, a parametric study is carried out for the response of three types of common structural forms under the effect of time-harmonic loading. We should also note that we only need the equivalent stiffness matrix from the half-space and there is no need to impose any boundary conditions on the equivalent stiffness matrix.

Validation

A Cube with Distributed Time-Harmonic Loading

In this part, a cubic structure is analyzed under some external tractions and the output is compared with the results of ABAQUS. To do so, a cube shown in Figure 2 with a dimension of 6 m in each side and filled by an isotropic material with mass density of $\rho = 100 \text{ Kg/m}^3$, shear modulus of $\mu = 10^6 \text{ N/m}^2$ and Poisson ratio of $\nu = 0.25$ is considered. The bottom and the vertical surface boundaries are restrained against movement in the normal direction. A time-harmonic distributed load with a magnitude of $p = 100 \text{ N/m}^2$ is applied on the top face of the cube. This problem has been solved with the use of the commercial software ABAQUS and the code written for the present work, where the results for the vertical displacement of the middle of the top face are shown in Figure 3. As seen, a perfect match is observed, which proves the validity and

accuracy of the codes written in this research for the FE part.

Circular Patch Loading

To test the validity and accuracy of the Boundary Element code and the Green’s functions used, we apply in turn a uniform vertical and horizontal time-harmonic circular patch load on the surface of the TIHS. The mesh used to model the loaded area is shown in Figure 4. For this type of boundary value problem, a semi-analytical solution is available in the literature (Rahimian et al., 2007). We define the dimensionless vertical and horizontal components of displacement as $[u_0, w_0] = \pi c_{44} a [u, w]$, where u and w are the vertical and horizontal components of the displacement and a is the radius of the circular patch load. The dimensionless frequency is also defined as $\omega_0 = a\omega\sqrt{\rho_s / c_{44}}$. We present the displacements for two groups of material constants as shown in Table 1. The engineering constants E, E', G, G', ν and ν' are related to the elastic constants c_{ij} according to Eq. (11). We also take $\omega_0 = 3$ in all cases.

As seen in Figures 5 and 6, there exists an excellent agreement between the numerical results obtained in this work and the analytical solutions available in the literature. This shows that the 4-point Gauss quadrature used in evaluation of the element integrals is adequate for the constant load distribution.

Table 1. Material constants used for verification of the BE code

Material Number	Material Constants					
	E (GPa)	E' (GPa)	G (GPa)	G' (GPa)	ν (GPa)	ν' (GPa)
1 (isotropic)	50	50	20	20	0.25	0.25
2	50	150	20	20	0.25	0.25

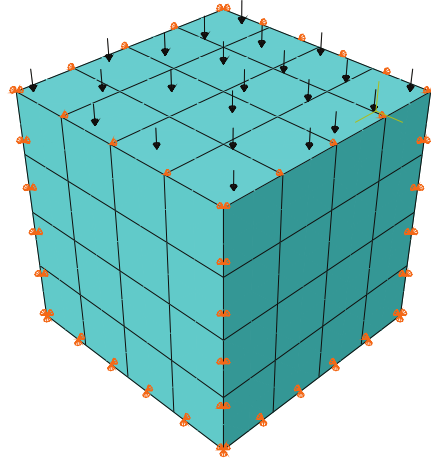


Fig. 2. The mesh of a cube with a dimension of 6 m used for verification of the FE code

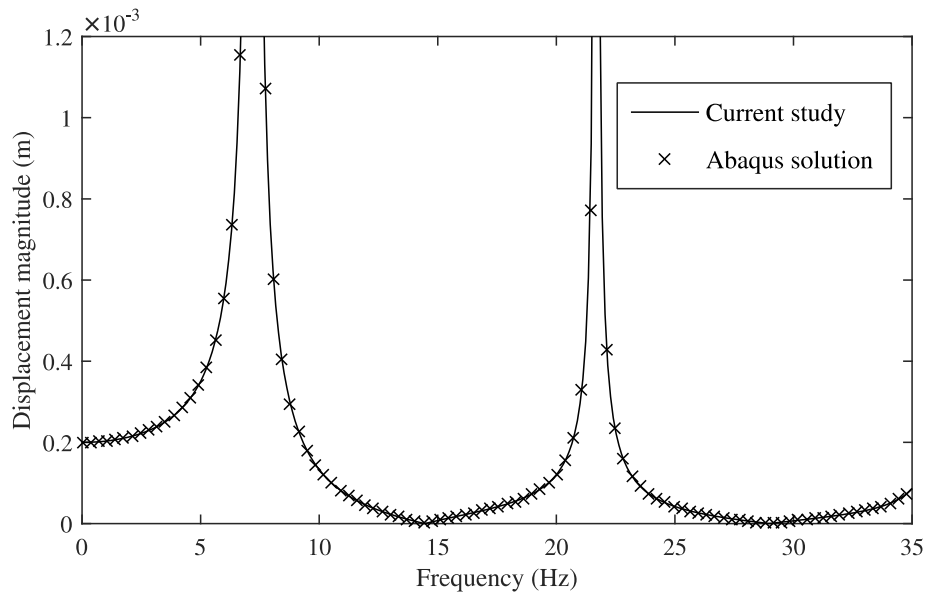


Fig. 3. Comparison of FE results from the current study and the commercial software ABAQUS

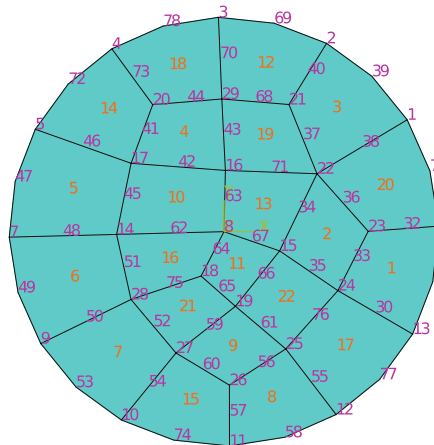


Fig. 4. The mesh for the loaded area on the surface of the THIS

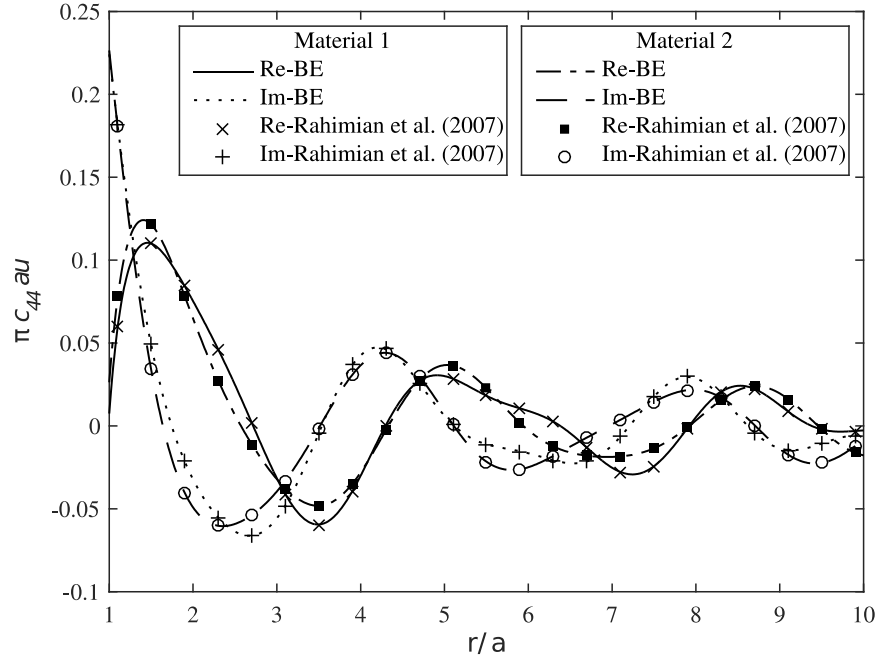


Fig. 5. Real and imaginary parts of dimensionless displacement in the horizontal direction when a uniform circular load is applied on the surface in the horizontal direction

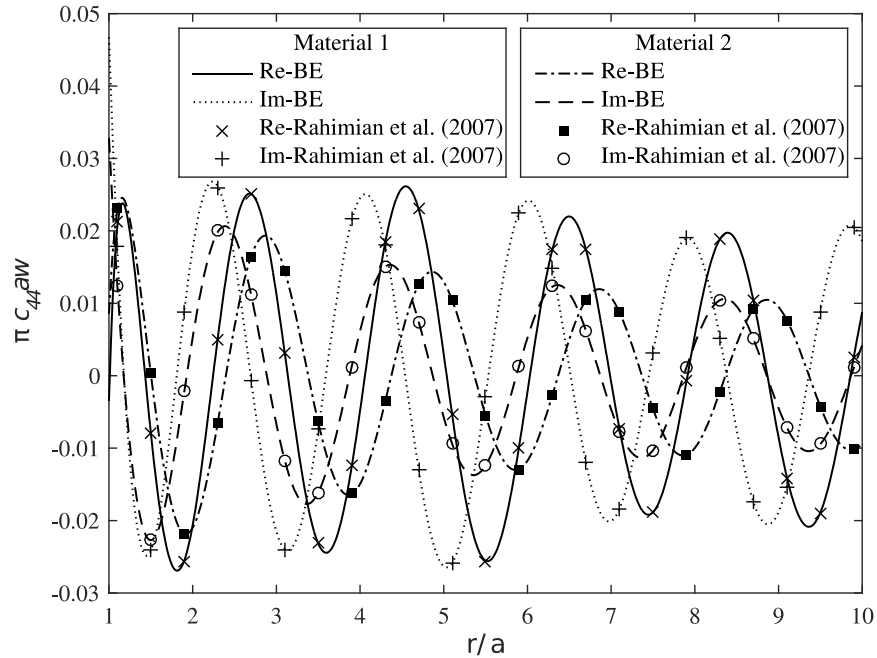


Fig. 6. Real and imaginary parts of dimensionless displacement in the z direction when a vertical uniform circular load is applied on the surface of the half-space

Rigid Square Foundation Bonded to an Isotropic Half-Space

In this section, the problem of interaction of a square rigid massless foundation bonded to the surface of an isotropic half-space is

investigated using the combined FE-BE program. The results of this investigation are compared with Guzina (2000) to show the accuracy of the numerical procedure used in this paper. To this end, a square foundation

with the length of $2b = 3$ m and a thickness of $h = 0.5$ m is considered. The elastic constants for the soil beneath this square foundation are defined as $E = 50$ MPa , $\nu = 1/3$ and $\rho_s = 2000$ Kg/m³ . An $8 \times 8 \times 2$ partition for the mesh is used to obtain the solution, which is displayed in Figure 7. A uniform distributed vertical force is applied on the top face of the foundation in order to determine the vertical impedance (K_{vv}) values. To this end, the vertical displacement of the rigid foundation is determined with the use of the combined FE-BE program as a base for calculating the impedance function. Figure 8 shows the results of this study and those of Guzina (2000), simultaneously. It is interesting to note that for the values of the dimensionless frequency greater than about 1.5, there exists almost an exact agreement compared with the results reported by Guzina (2000). This can be attributed to the fact that the nature of the singularity at the edges of the foundation changes as the frequency of excitation increases and also we expect generally a better performance from the quadratic isoparametric elements compared to the linear elements used in Guzina's research.

We can also carry out a convergence study for the stiffness values of a rectangular foundation in bonded contact with an isotropic half-space. Figure 9 depicts the values calculated by Guzina et al. and those obtained in the current study. Excellent agreement is observed for each mesh that was considered.

Massive Circular Foundations on the Surface of the Half-Space

In this section, we consider the vertical vibrations of a rigid massive circular foundation in contact with an isotropic medium as the last example for verification. Analytical solutions for this problem can be found in references such as Awojobi and Grootenhuis (1965) and Richart et al. (1970). These solutions were derived by assuming the traction distribution beneath the foundation to be the same as the static case. The dimensionless mass ratio is defined as $q = m / (\rho_s a^3)$, where m is the total mass of the circular foundation, ρ_s is the density of the soil medium and a is the foundation radius. Figure 11 shows the solution over a dimensionless frequency range of 0~1.6 and for several values of the dimensionless mass ratio. The mesh used is also depicted in Figure 10.

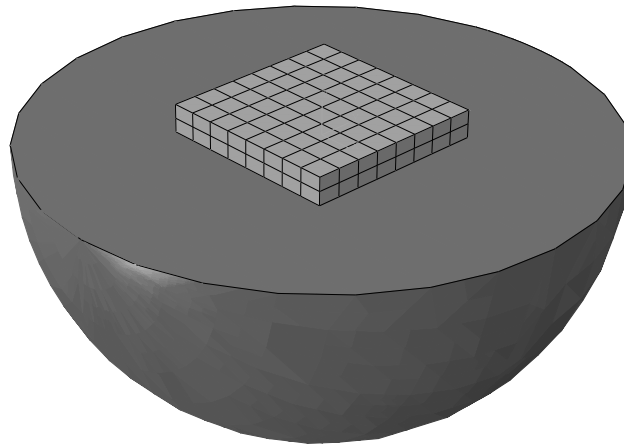


Fig. 7. The $8 \times 8 \times 2$ mesh of the square foundation and a portion of the half-space

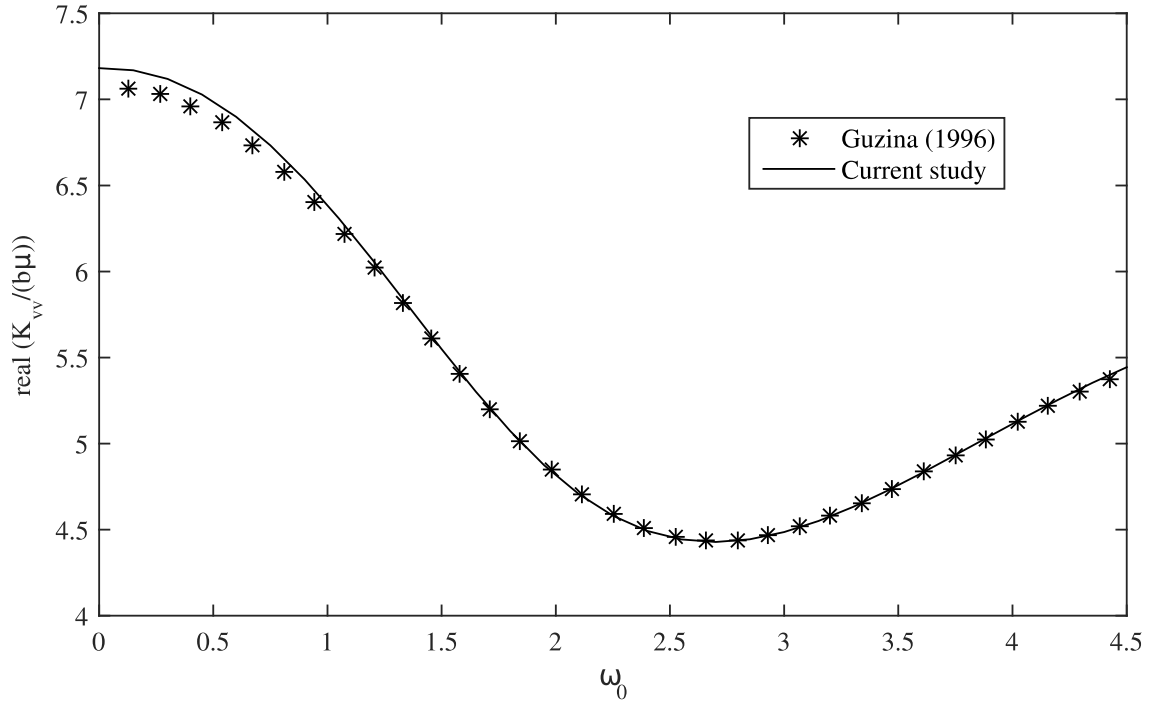


Fig. 8. Comparison of the real part of the vertical impedance values for a rigid square foundation with those of Guzina (1996)

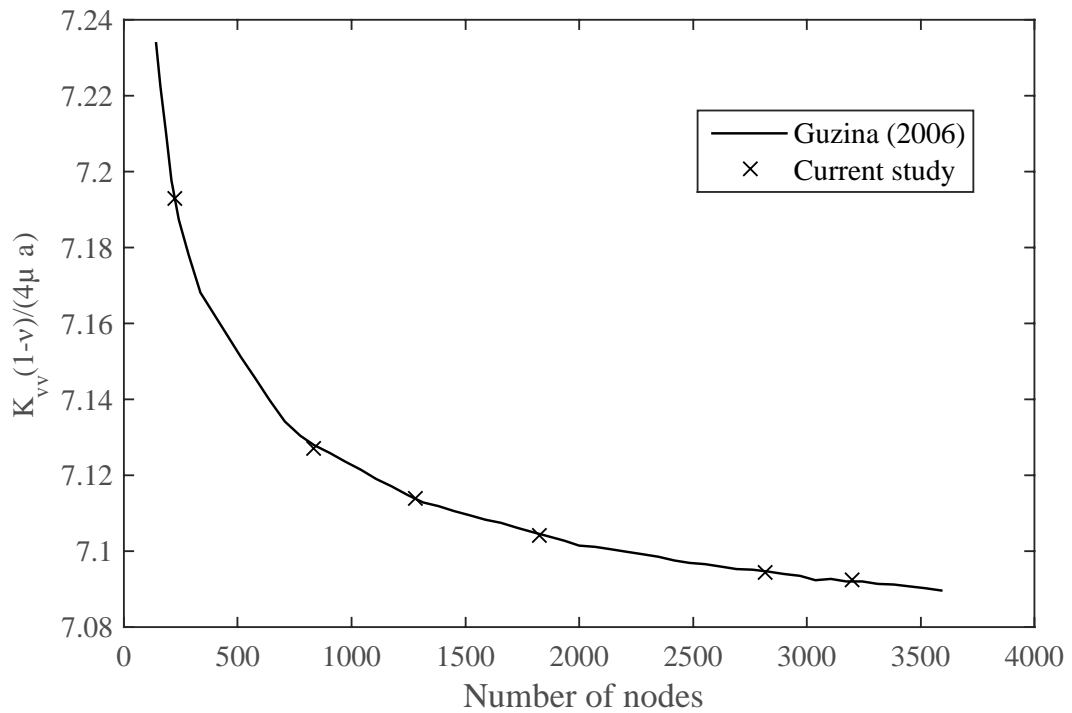


Fig. 9. Convergence of the dimensionless stiffness values with increasing the number of nodes in the mesh

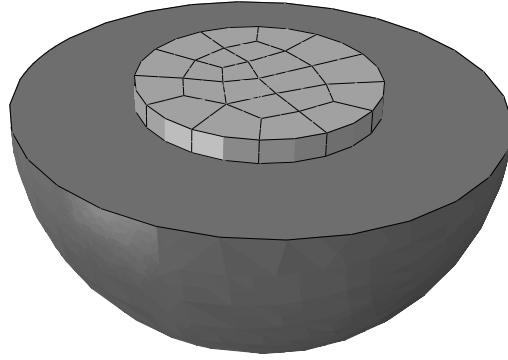


Fig. 10. The mesh of the circular foundation and a portion of the half-space

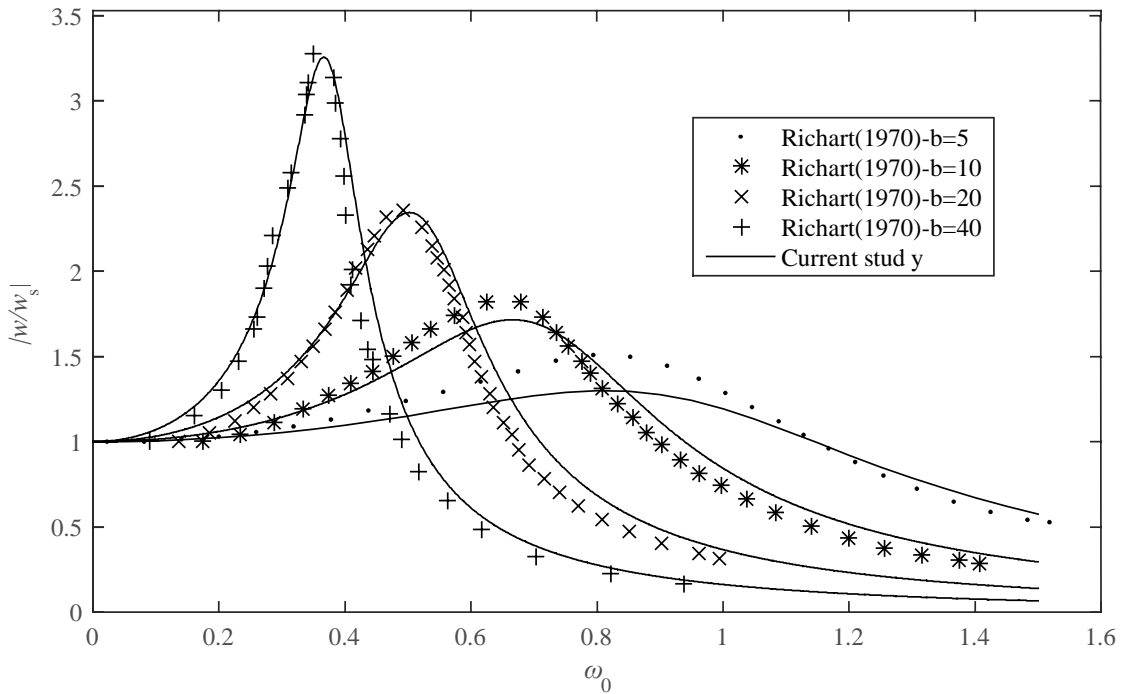


Fig. 11. Relative displacements for circular foundations with different mass ratios

The results follow the expected trend as the values of dimensionless frequency increases. A good match is also recognized for the higher values of the dimensionless mass ratio and the existing discrepancy can be attributed to the following reasons:

1. The solutions in Richart et al. (1970) have been derived with the assumption that the distribution of tractions under the foundation for the dynamic case is the same as that obtained for the static case.

2. The solution in the current study is for the bonded case, while those of the analytical solution are presented for the simpler problem of frictionless contact, and they are not exactly the same.

3. The usual approximations associated with a numerical solution such as: a) numerical Gauss integration used over each element; b) approximations introduced by discretization of the domain; c) numerical

computation of the Hankel integrals. These approximations make some small error.

4. Errors associated with conversion of the graph in Richart et al. (1970) to numbers that could be used for comparison.

Parametric Study

In the following sections, we investigate the effects of transverse isotropy of the elastic half-space on the dynamic response of three different types of not necessarily rigid superstructure, which are circular or square flexible foundations and a more general type of massive structure. In all these applications, the materials for TIHS are chosen from Table 2. In this table Material 1 is for an isotropic material and is chosen as a reference for evaluation of the effect of the degree of anisotropy. Compared with the reference isotropic material, Materials 2 and 3 are selected to have larger values of E and G , while Materials 4 and 5 have larger values for E' and Materials 6 and 7 have smaller values for G' .

Circular and Square Flexible Foundations

Consider a flexible circular foundation with a radius of $a=1.5$ m and elastic constants $E = 20$ GPa, $\nu = 0.2$ and $\rho_f = 2400$ Kg/m³ bonded to the surface of a transversely isotropic half-space filled by one of the materials listed in Table 2. Figures 12-14 show the vertical displacement of the central point of the foundation in terms of dimensionless frequency and different

variation of elastic constants when a distributed load of 10 kN is applied on its upper surface.

An interesting observation in the results for the circular foundation is that by increasing E or E' , the absolute value of both the real and imaginary parts of displacement decrease before the nondimensional frequency of 1.5. For the real part, this trend is reversed for nondimensional frequencies larger than 1.5, when E' increases. Moreover, the effect of increasing E' is much more significant on both the real and imaginary parts of displacement. This means that whenever $E'/E > 1$ it is more important to take the anisotropy into consideration.

As it is observed in Figures 15-17, for the rectangular foundation, the general behavior is similar to the circular foundation. However, when E' is increased, the reversal of the direction of change for the real part does not happen in the frequency range 0~4 anymore.

Analysis of a General Structure

Figure 18 depicts the vertical section of a common type of concrete structure for a reactor building. We consider three types of models with different geometric dimensions as stated in Table 3. The material constants for the concrete are taken as $E = 30$ GPa, $\nu = 0.2$ and $\rho = 2400$ Kg/m³ and the materials for the soil are selected from the list described in Table 2.

Table 2. Materials chosen for the parametric study

Material	Elastic Parameters							
	E (MPa)	E' (MPa)	G (MPa)	G' (MPa)	ν	ν'	E'/E	G'/G
Mat 1	50	50	20	20	0.25	0.25	1.0	1.0
Mat 2	100	50	40	20	0.25	0.25	0.5	1/2
Mat 3	150	50	60	20	0.25	0.25	1/3	1/3
Mat 4	50	100	20	20	0.25	0.25	2.0	1.0
Mat 5	50	150	20	20	0.25	0.25	3.0	1.0
Mat 6	50	50	20	10	0.25	0.25	1	1/2
Mat 7	50	50	20	5	0.25	0.25	1	1/4

Table 3. Dimension parameters for different models

Geometry	H (m)	D (m)	R (m)	t (m)
Model 1	28.0	60.0	28.0	2.2
Model 2	45.0	50.0	22.5	2.0
Model 3	55.7	70.0	28.0	2.5

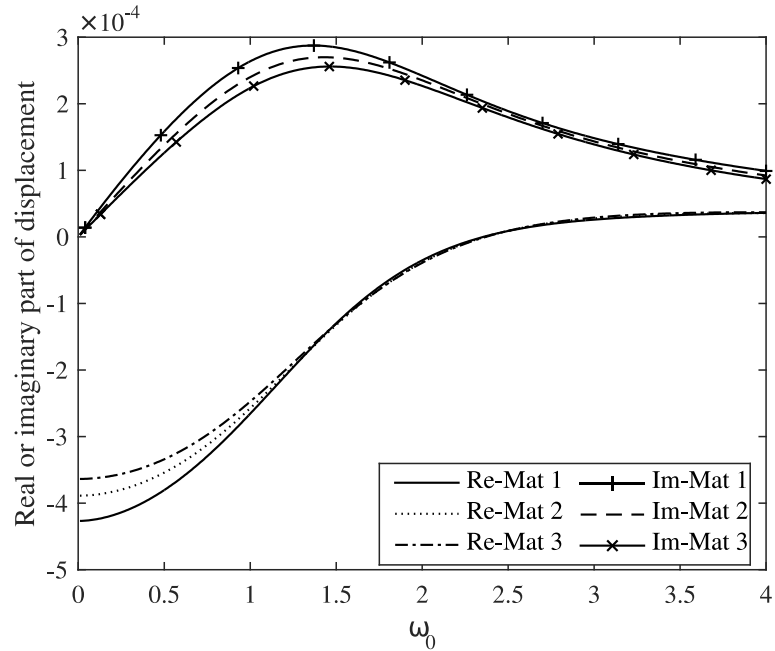


Fig. 12. Real and imaginary part of the vertical displacement of the central point of the circular flexible foundation when E varies

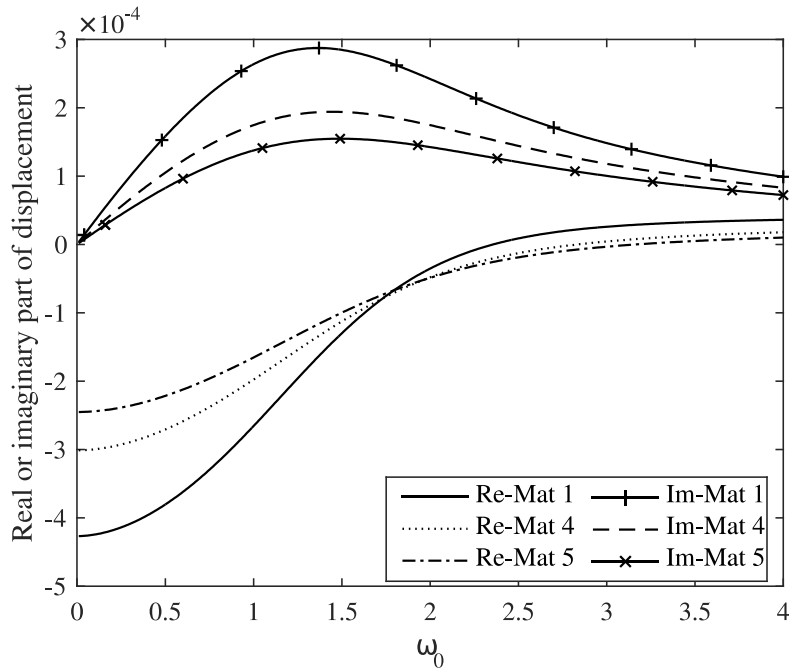


Fig. 13. Real and imaginary part of the vertical displacement of the central point of the circular flexible foundation when E' varies

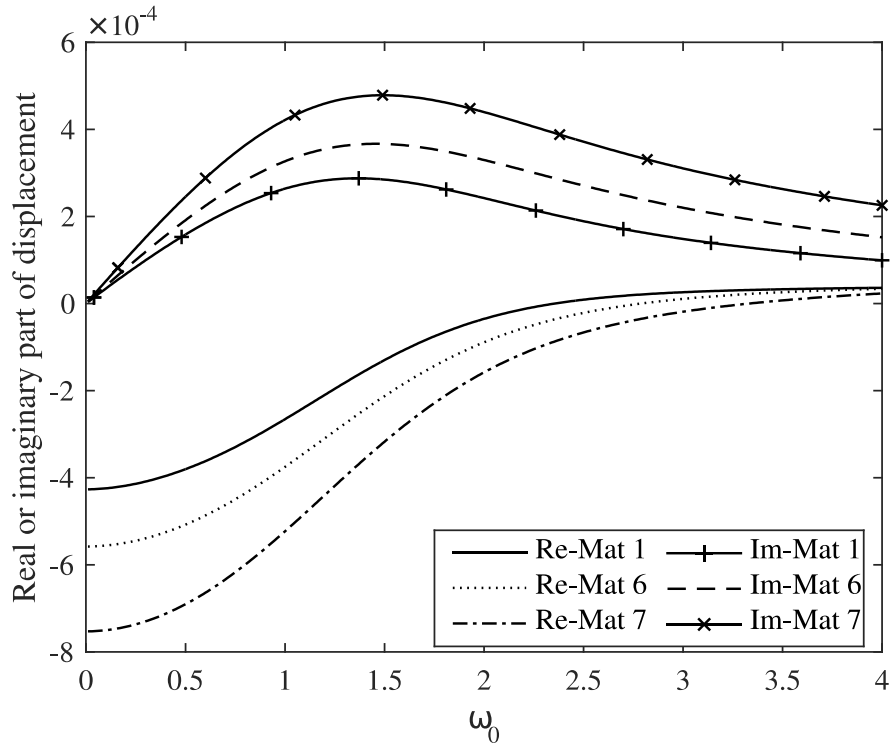


Fig. 14. Real and imaginary part of the vertical displacement of the central point of the circular flexible foundation when G' varies

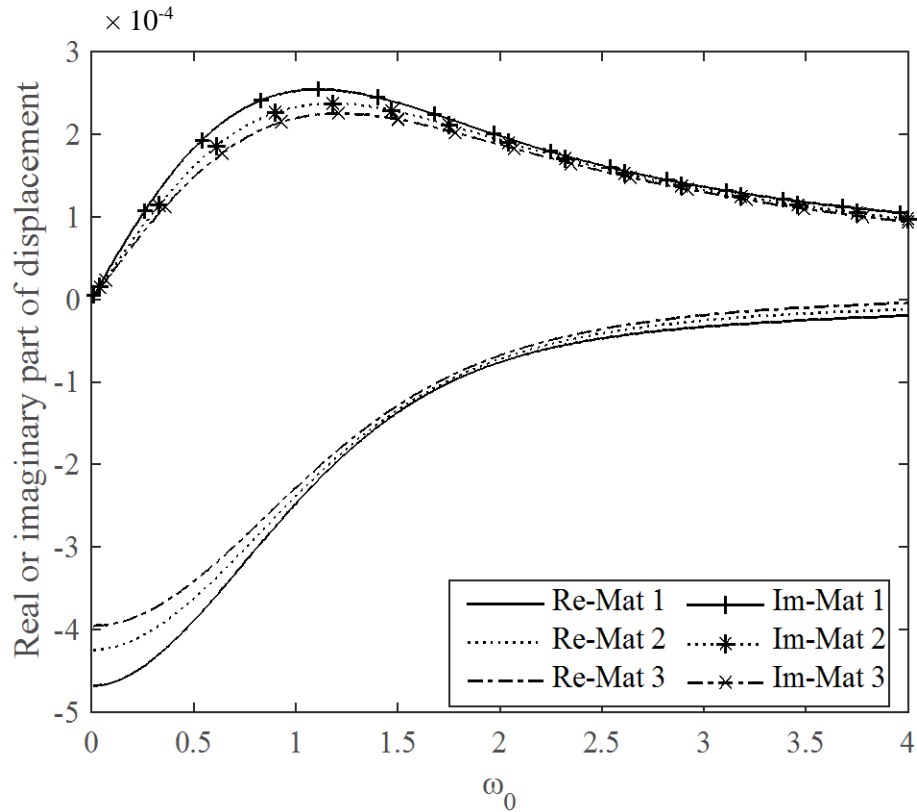


Fig. 15. Real and imaginary part of the vertical displacement of the central point of the rectangular flexible foundation when E varies

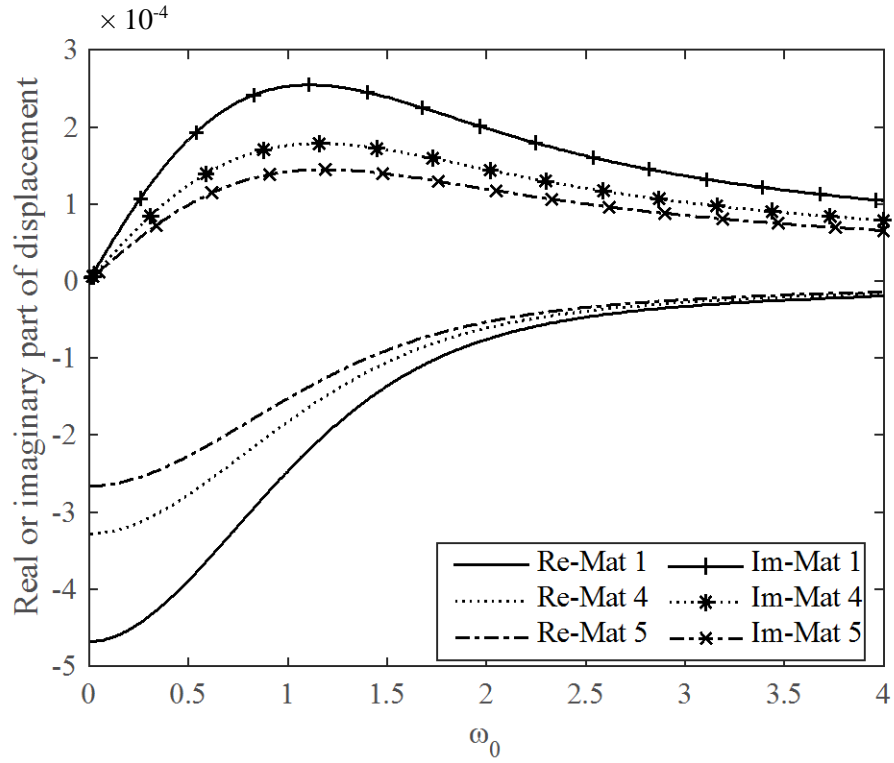


Fig. 16. Real and imaginary part of the vertical displacement of the central point of the rectangular flexible foundation when E' varies

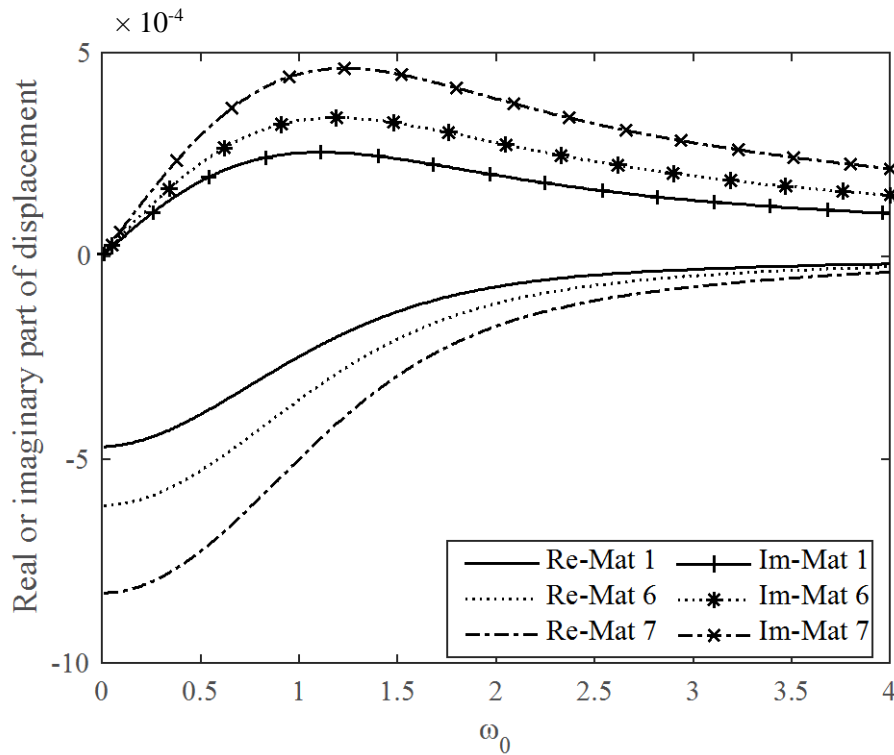


Fig. 17. Real and imaginary part of the vertical displacement of the central point of the rectangular flexible foundation when G' varies

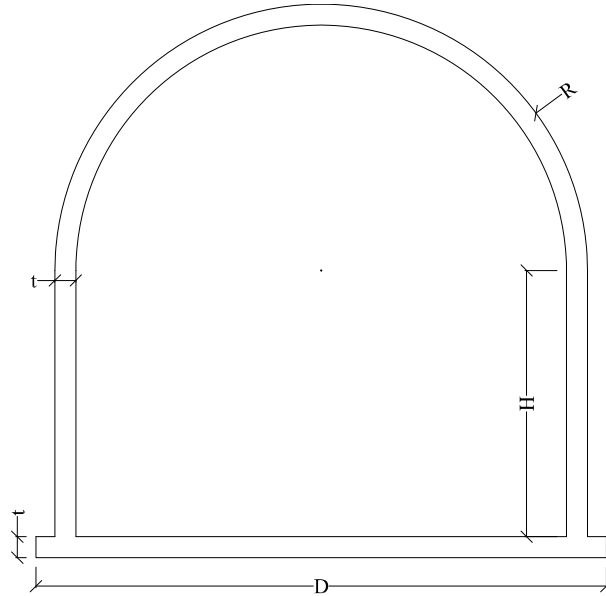


Fig. 18. Vertical plan of a typical concrete structure

To investigate the response of the structure, a time-harmonic horizontal point load equal to 10 kN is applied on the top of the structure at point A. To observe the effects of taking the soil medium into consideration, we first present the results for the case, where the degrees of freedom on the bottom surface of the structure are constrained against movement in every direction, which describes a rigid base for the structure, as it is modeled in ordinary structural analysis. The results in Figure 19 are presented for a frequency range of 15~45 rad/sec. From this figure, we can extract the values of the natural vibration frequency of the structure. These values can of course be obtained using a simple eigenvalue analysis when the bottom of the structure is clamped. However, such an analysis is not possible when taking the underlying soil into account. Thus, we extract them from the graphs. As expected, the height of the structure plays an important role and as the height of the structure increases, the fundamental frequency of the structure decreases.

Figures 20-22 illustrate the magnitude of maximum horizontal displacement of the structure when the soil medium is taken into

consideration in the FE-BE code. The plots demonstrate how the dynamic behavior changes when each of the elastic parameters change for different models.

The period ($T = 2\pi / \omega$) for each model and for different materials has been listed in Table 4. The following observations can be made after a detailed analysis of this table and the graphs in Figures 20-22:

1- A change in values of E does not have a significant effect on the maximum values of displacement and mainly affects the period of the structure.

2- Increasing the height of the structure results in an increase in the period, however the geometric parameter that has the most significant effect on the maximum displacement magnitude is the area of the foundation in contact with the TIHS. This is why the graphs for Model 2 lie between those of the first and third model.

3- As the frequency of the excitation increases, the displacement values converge to a unique value for all of the materials considered.

4- The dynamic response is more sensitive to a variation in values of E' and G' than a change in values of E , which means that the

degree of anisotropy defined as either E'/E or G'/G is the more significant parameter.

5- Taking SSI into account has a more dramatic effect on structures with higher

periods. However, the consideration of transverse isotropy seems to have a more significant effect on structures with lower periods.

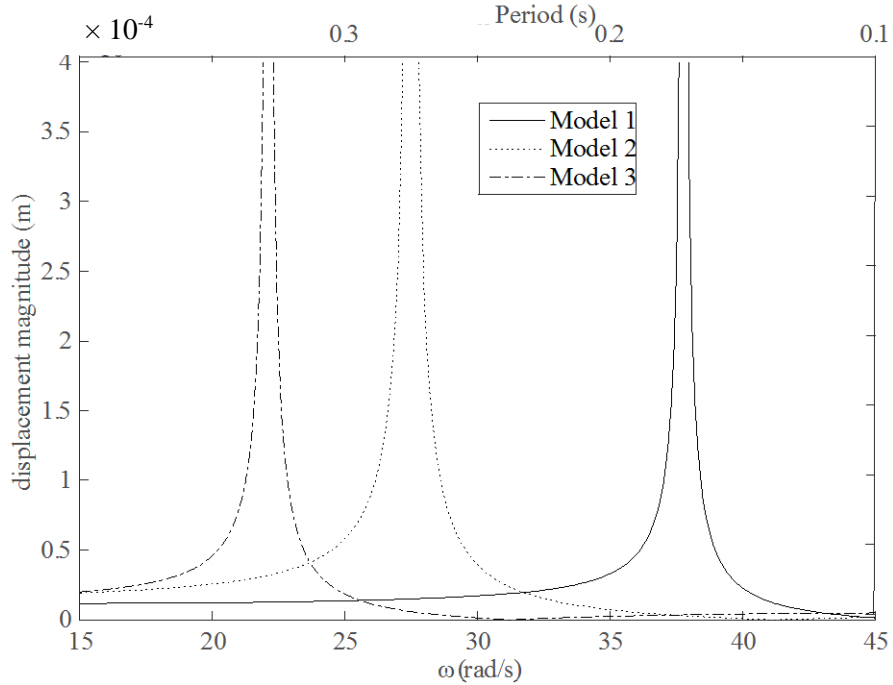


Fig. 19. Maximum displacement for the three models in the vicinity of the first fundamental vibration frequency

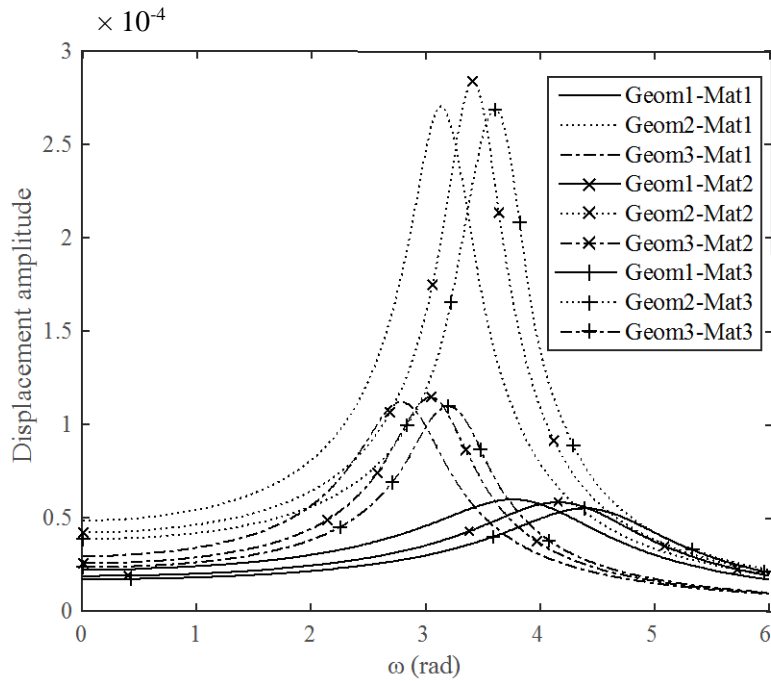


Fig. 20. Maximum displacement magnitude when E changes for each model

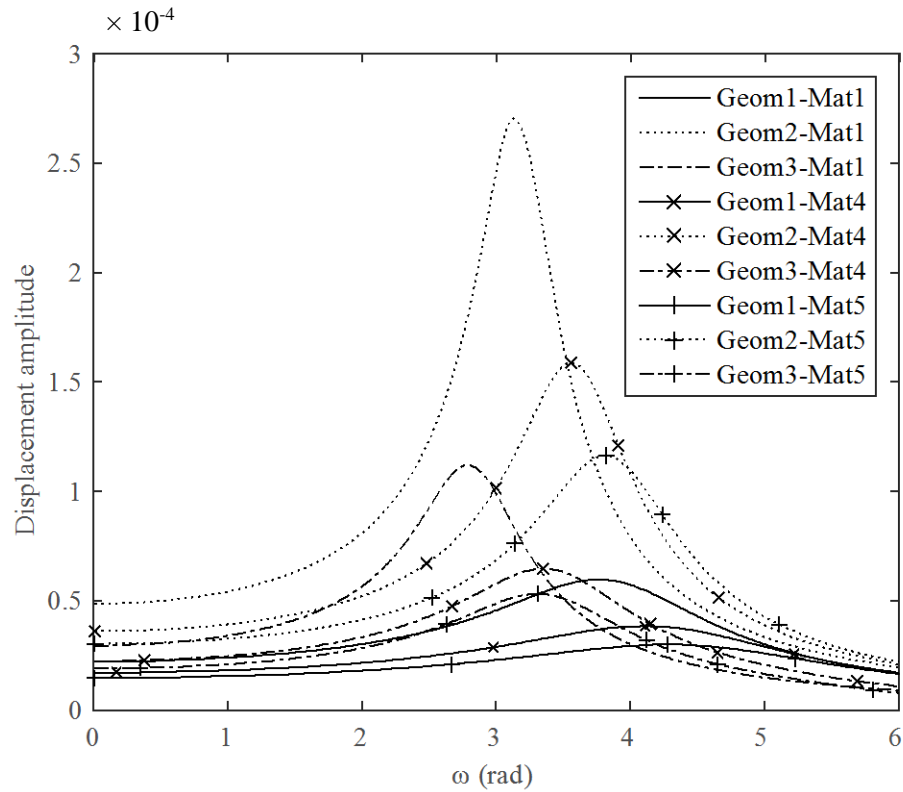


Fig. 21. Maximum displacement magnitude when E' changes for each model

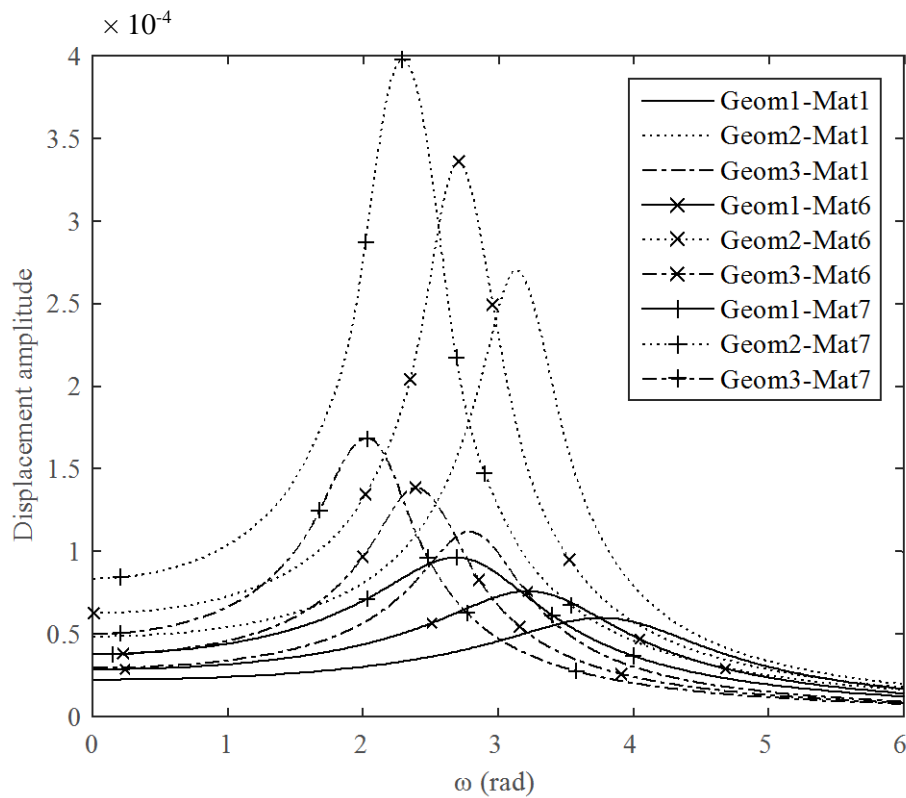


Fig. 22. Maximum displacement magnitude when G' changes for each model

Table 4. Periods of the structures on different materials (seconds)

Model	Material							Clamped
	1	2	3	4	5	6	7	
Model 1	1.64	1.51	1.43	1.56	1.49	1.98	2.34	0.166
Model 2	2.02	1.84	1.71	1.81	1.63	2.34	2.85	0.229
Model 3	2.30	2.05	1.90	1.91	1.91	2.66	2.96	0.274

CONCLUSIONS

In this paper, the dynamic analysis of general 3D structures bonded to the surface of a transversely isotropic medium has been addressed. The structure has been modeled using the Finite Element method with 20-node isoparametric brick elements. A conforming mesh of 8-node quadratic elements on the surface of the half-space has been considered for the Boundary Element analysis of the transversely isotropic half-space. The BE procedure uses half-space Green's functions for a transversely isotropic medium, the formulation of which has been presented in a concise form. The matrices computed for the half-space have been converted using appropriate techniques and assembled with the structure's stiffness matrix. Using the program written for this paper, several verifications were carried out using some well-known examples from the literature. Finally, the effect of transverse isotropy has been studied for three different types of structures and the results have been presented for several materials and models. The results show that anisotropy of the soil medium can have significant effects on the dynamic behavior of the structure and since in natural soil deposits, this behavior is the norm rather than the exception, its inclusion is highly recommended.

ACKNOWLEDGEMENT

The partial support from the University of Tehran through 27840/1/08 to the second author during this work is gratefully acknowledged.

NOTATION

- C** Structure's damping matrix
- E** Young's modulus in plane of transverse isotropy
- E'** Young's modulus normal to plane of transverse isotropy
- G** Matrix of influence coefficients
- G** Shear modulus in planes normal to the axis of symmetry
- G'** Shear modulus in planes normal to plane of transverse isotropy
- I** Identity matrix
- I_q ($q = 1, 2, \dots, 6$) Integrals present in the fundamental solutions
- $J_n(x)$ Bessel's function of first kind and order n
- K** Structure's stiffness matrix
- K_b** Soil stiffness matrix
- K_f(ω)** Dynamic stiffness matrix
- M** Structure's mass matrix
- Q** A matrix relating nodal tractions to nodal equivalent forces
- T** Transformation matrix
- a Radius of circular path and foundation
- c_{ij} ($i, j = 1, 2, 3$) Elasticity constants
- c^i Smoothness matrix
- f** Nodal equivalent forces
- m Total mass of the foundation
- p** Nodal tractions
- $\hat{\mathbf{p}}$ Global nodal tractions (on the BE boundary)
- $\mathbf{p}^{*i}(\mathbf{x}, \omega)$ Traction Green's tensor
- q Dimensionless mass ratio
- r Radial component in the cylindrical coordinate system
- u** Displacement vector

$\dot{\mathbf{u}}$	Velocity vector
$\ddot{\mathbf{u}}$	Acceleration vector
$\hat{\mathbf{u}}$	Global nodal displacements (on the BE boundary)
$\mathbf{u}^{*i}(\mathbf{x}, \omega)$	Displacement Green's tensor
u_{ij}	Displacement in j direction when a point load is applied in the i direction
\mathbf{x}	Position vector
Γ_b	Boundary of the domain modeled by BEM
Γ_l	The shared boundary between the BE and the FE regions
Φ	Matrix of shape functions
Ω_b	The TIHS' domain
Ω_f	Structure's domain
θ	Angular component in the cylindrical coordinate system
μ	Lamé constant
ν	Poisson's ratio in the plane of transverse isotropy when the loading is in the same plane
ν'	Poisson's ratio in the plane of transverse isotropy when the loading is normal to the plane of transverse isotropy
ξ	Hankel's parameter
ρ	Density
ω	Frequency of excitation
ω_0	Dimensionless frequency

REFERENCES

- Akbari, F., Khojasteh, A., Rahimian, M. (2016), "Three-dimensional interfacial Green's function for exponentially graded transversely isotropic bi-materials", *Civil Engineering Infrastructures Journal*, 49(1), 71-96.
- Aleynikov, S.M. (2010). *Spatial contact problems in geotechnics*, Boundary Element method, Springer.
- Amiri-Hezaveh, A., Eskandari-Ghadi, M., Rahimian, M. and Ghorbani-Tanha, A.K. (2013). "Impedance functions for surface rigid rectangular foundations on transversely isotropic multilayer half-spaces", *Journal of Applied Mechanics* 80(5), 051017.
- Ardeshir-Behrestaghi, A., Eskandari-Ghadi, M. and Vaseghi-Amiri, J. (2013). "Analytical solution for a two-layer transversely isotropic half-space affected by an arbitrary shape dynamic surface load", *Civil Engineering Infrastructures Journal*, 1(1), 1-14.
- Awojobi, A.O. and Grootenhuys, P. (1965). "Vibration of rigid bodies on semi-infinite elastic media", *Proceedings of the Royal Society A: Mathematical, Physical and Engineering Sciences*, 287(1408), 27-63.
- Baziar, M.H. and Song, C. (2006). "Time-harmonic response of non-homogeneous elastic unbounded domains using the scaled Boundary Finite Element method", *Earthquake Engineering and Structural Dynamics*, 35(3), 357-383.
- Chen, R. and An, C. (2014). "On the evaluation of infinite integrals involving Bessel functions", *Applied Mathematics and Computation*, 235, 212-20.
- Coulier, P., François, S., Lombaert, G. and Degrande, G. (2014). "Coupled Finite Element – hierarchical Boundary Element methods for dynamic soil – structure interaction in the frequency domain", *International Journal for Numerical Methods in Engineering*, 97(7), 505-530.
- Elleithy, W. and Al-Gahtani, H.J. (2000). "An overlapping domain decomposition approach for coupling the Finite and Boundary Element methods", *Engineering Analysis with Boundary Elements*, 24(5), 391-98.
- Elleithy, W.M., Al-Gahtani, H.J. and El-Gebeily, M. (2001). "Iterative coupling of BE and FE methods in elastostatics", *Engineering Analysis with Boundary Elements*, 25(8), 685-695.
- Eskandari-Ghadi, M. (2005). "A complete solution of the wave equations for transversely isotropic media", *Journal of Elasticity*, 81(1), 1-19.
- Eskandari-Ghadi, M. and Amiri-Hezaveh, A. (2014). "Wave propagations in exponentially graded transversely isotropic half-space with potential function method", *Mechanics of Materials*, 68, 275-292.
- Eskandari-Ghadi, M. and Ardeshtir-Behrestaghi, A. (2010). "Forced vertical vibration of rigid circular disc buried in an arbitrary depth of a transversely isotropic half-space", *Soil Dynamics and Earthquake Engineering*, 30(7), 547-560.
- Eskandari-Ghadi, M., Ardeshtir-Behrestaghi, A., Pak, R.Y.S., Karimi, M. and Momeni-Badeleh, M. (2013). "Forced vertical and horizontal movements of a rectangular rigid foundation on a transversely isotropic half-space", *International Journal for Numerical and Analytical Methods in Geomechanics*, 37(14), 2301-2320.
- Eskandari-Ghadi, M., Gorji-Bandpey, G., Ardeshtir-Behrestaghi, A. and Nabizadeh, S.M. (2015). "Tensionless-frictionless interaction of flexible annular foundation with a transversely isotropic multi-layered half-space", *International Journal for Numerical and Analytical Methods in*

- Geomechanics*, 39(2), 155-174.
- Eskandari-Ghadi, M., Hasanpour-Charmhini, A. and Ardeshir-Behrestaghi, A. (2014). "A method of function space for vertical impedance function of a circular rigid foundation on a transversely isotropic ground", *Civil Engineering Infrastructures Journal*, 47(1), 13-27
- Eskandari-Ghadi, M., Pak, R.Y.S. and Ardeshir-Behrestaghi, A. (2012). "Vertical action of a concentric multi-annular punch on a transversely isotropic elastic half-space", *Journal of Applied Mechanics*, 79(4), 41008.
- Frangi, A. and Novati, G. (2003). "BEM-FEM coupling for 3D fracture mechanics applications", *Computational Mechanics*, 32(4-6), 415-422.
- Givoli, D. (2004). "High-order local non-reflecting boundary conditions: A review", *Wave Motion* 39(4), 319-326.
- Gucunski, N. and Peek, R. (1993). "Vertical vibrations of circular flexible foundations on layered media", *Soil Dynamics and Earthquake Engineering*, 12(3), 183-192.
- Hamidzadeh a, B.B. (1996). "Seismic response of foundations and structures in multilayered media", Ph.D. Thesis, University of Colorado.
- Hamidzadeh, H.R., Dai, L. and Jazar, R.N. (2014). *Wave propagation in solid and porous half-space media*, Springer.
- Hematiyan, M.R., Khosravifard, A. and Mohammadi, M. (2012). "A general technique for coupling two arbitrary methods in stress analysis", *International Journal of Computational Methods*, 9(2), 1240027.
- Kokkinos, F.T. and Spyrakos, C.C. (1991). "Dynamic analysis of flexible strip-foundations in the frequency domain", *Computers and Structures*, 39(5), 473-482.
- Li, M., Lu, X., Lu, X. and Ye, L. (2014). "Influence of soil-structure interaction on seismic collapse resistance of super-tall buildings", *Journal of Rock Mechanics and Geotechnical Engineering*, 6(5), 477-485.
- Lima, M.V.A., Lima, J.M.F. and Lima, P.R.L. (2014). "Finite Difference energy method for nonlinear numerical analysis of reinforced concrete slab using simplified isotropic damage model", *Revista IBRACON de Estruturas e Materiais*, 7(6), 940-964.
- Lu, Y.Y., Belytschko, T. and Liu, W.K. (1991). "A variationally coupled FE-BE method for elasticity and fracture-mechanics", *Computer Methods in Applied Mechanics and Engineering*, 85(1), 21-37.
- Luco, J.E. and Westmann, R.A. (1971). "Dynamic response of circular footings", *Journal of Engineering Mechanics, ASCE*, 97(5), 1381-1395.
- Nielsen, A.H. (2014). "Towards a complete framework for seismic analysis in abaqus", *Proceedings of the ICE - Engineering and Computational Mechanics*, 167(1), 3-12.
- Rahimian, M., Eskandari-Ghadi, M., Pak, R.Y.S. and Khojasteh, A. (2007). "Elastodynamic potential method for transversely isotropic solid", *Journal of Engineering Mechanics*, 133(10), 1134-1145.
- Richart, F.E., Hall, J.R. and Woods, R.D. (1970). *Vibration of soils and foundations*, Prentice-hall, Englewood Cliffs, New Jersey.
- Savadatti, S. and Guddati, M.N. (2012a). "Accurate absorbing boundary conditions for anisotropic elastic media, Part 1: Elliptic anisotropy", *Journal of Computational Physics*, 231(22), 7584-7607.
- Savadatti, S. and Guddati, M.N. (2012b). "Accurate absorbing boundary conditions for anisotropic elastic media, Part 2: Untitled non-elliptic anisotropy", *Journal of Computational Physics*, 231(22), 7608-7625.
- Soares, D. and Godinho, L. (2014). "An overview of recent advances in the iterative analysis of coupled models for wave propagation", *Journal of Applied Mathematics*, Jan., 1-21.
- Whittaker, W.L. and Christiano, P. (1982). "Dynamic response of plates on elastic half-space", *Journal of Engineering Mechanics Division, ASCE*, 108(1), 133-154.
- Wong, H.L. and Luco, J.E. (1976). "Dynamic response of rigid foundations of arbitrary shape", *Earthquake Engineering and Structural Dynamics*, 4(6), 579-587.
- Yazdchi, M., Khalili, N. and Valliappan, S. (1999). "Dynamic soil-structure interaction analysis via coupled Finite Element-Boundary Element method", *Soil Dynamics and Earthquake Engineering*, 18(7), 499-517.
- Zienkiewicz, O.C., Kelly, D.W. and Bettess, P. (1977). "The coupling of the finite element method and boundary solution procedures", *International Journal for Numerical Methods in Engineering*, 11(2), 355-375.
- Zienkiewicz, O.C., Taylor, R.L. and Zhu, J.Z. (2013). *The Finite Element method: Its basis and fundamentals*, Elsevier.